JOURNAL OF CATALYSIS 98, 204–220 (1986)

# Ammoxidation of 3-Picoline: An Activity and High-Resolution Electron Microscopic Investigation of Vanadium Oxide Catalysts

ARNE ANDERSSON,* JAN-OLOV BOVIN,† AND PAUL WALTER†

*Department of Chemical Technology and †Department of Inorganic Chemistry 2, Chemical Center, Lund Institute of Technology, P.O. Box 124, S-221 00 Lund, Sweden

Received February 8, 1985; revised September 16, 1985

A $V_2O_5$ catalyst was used in the ammoxidation of 3-picoline to nicotinonitrile. It was observed that the selectivity for the formation of $CO_2$ as a function of temperature passed through a minimum. This is explained to be due to the existence of weakly bonded electrophilic oxygen species at low temperatures, and an increasing degradation involving $O^{2-}$ at high temperatures. A comparison of two different $V_2O_5$ preparations shows the beneficial effect of the $V_2O_5$(010) plane on the formation of nicotinonitrile. The exposure of planes other than the (010) plane as the source of formation of $CO_2$ is discussed by consideration of bond strength values. The activity, selectivity, and composition of the charged $V_2O_5$ catalyst were followed as a function of time-on-stream at various temperatures. It was found that the $V_2O_5$ phase was reduced in the course of the reaction. $V_4O_9$, $VO_2$(B), $VO_2$ (tetragonal), and even more reduced phases were formed depending upon the reaction temperature used. Of the pure oxides, $V_4O_9$ was found to be both less active and less selective than $V_2O_5$. $VO_2$(B), however, is more active but less selective compared to $V_2O_5$. The phases formed were characterized by various methods including high-resolution transmission electron microscopy (HRTEM). This technique made it possible to image the $V_2O_5/V_4O_9$ phase boundary for the first time. The general direction of this boundary is parallel to the (301) plane of $V_2O_5$. Micrographs of $VO_2$(B) show that the nature of defects formed depends on the reaction temperature. After use at 695 K two types of planar twin lamellae were formed. At a slightly higher temperature partly amorphous defects appeared. The influence on the catalytic reaction of the phase boundaries and defects formed is discussed. 

## INTRODUCTION

The ammoxidation of 3-picoline to nicotinonitrile is of interest since the nitrile can be further transformed either to nicotinamide, a component of the vitamin B group, or to the provitamin nicotinic acid (Scheme 1). Both compounds are of importance for the metabolism of human beings and animals, and are used as food additives. The manufacture of nicotinamide via ammoxidation of 3-picoline is of great industrial interest, especially for developing countries. Yields between 80 and 90% for the production of nicotinonitrile and as high as 98–100% for the hydrolysis to nicotinamide have been reported in patents (*1*).

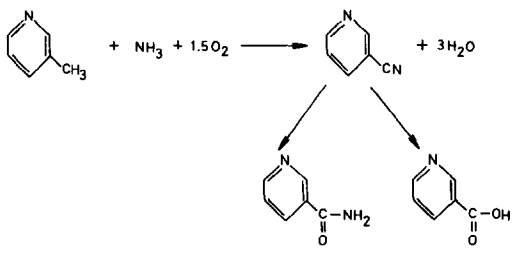


SCHEME 1

Vanadium oxide-based catalysts are generally used in the oxidation and ammoxidation of aromatic hydrocarbons. It is believed that lattice oxygen is consumed in the selective reaction, and that the reduced catalyst surface is reoxidized by molecular oxygen (*2*). The phase composition of the vanadium oxide catalyst in the stationary state depends on the composition of the reactant feed and on the temperature. The catalyst composition along the bed in plug flow reactors also varies (*3*). A previous in-



0021-9517/86 $3.00

vestigation of the ammoxidation of 3-picoline over $V_2O_5$, $V_6O_{13}$, and $VO_2$ (rutile) has shown that $V_6O_{13}$ is both highly active and selective (*4*). The same conclusion has been drawn in studies of the oxidation of propylene (*5*) and *o*-xylene (*6*). The eventual importance of $V_2O_5/V_6O_{13}$ phase boundaries for activity and selectivity in catalytic oxidation has already been suggested by Colpaert (*5*). The existence of such boundaries has also been used as an explanation for the performance of vanadium oxide catalysts in the ammoxidation of 3-picoline (*3, 4, 7*). Recently, it has been shown that it is not the phase boundary as such which is most active and selective, but a nonstoichiometric defect structure of $V_6O_{13}$ (*8*). Concerning $VO_2$ (rutile) contradictory results have been obtained. It has been concluded that in the ammoxidation of 3-picoline (*4*) and in the oxidation of *o*-xylene (*9*) this phase is not active. However, it was found to be active but nonselective in the oxidation of propylene (*5*). In the oxidation of naphthalene $V_2O_4$ showed some activity and selectivity (*10*).

Phase compositions with a stoichiometry between $V_2O_5$ and $VO_2$ are usually formed in catalytic oxidation and ammoxidation. In addition to the $V_2O_5$, $V_6O_{13}$, and tetragonal $VO_2$ phases, phases with compositions $V_3O_7$ (*11*), $V_4O_9$ (*12*), and $VO_2$(B) (*13*) also exist within this range. The crystal structures of $V_4O_9$ and $VO_2$(B) have not yet been verified. In the oxidation of tetrahydrofuran at 473 K, $V_4O_9$ was formed (*14*). Both $V_4O_9$ and $V_6O_{13}$ appeared when $V_2O_5$ single crystals, exposing vanadyl oxygen species, were used in the oxidation of propylene. The same experiment showed that these phases were selective for the formation of acrolein (*15*). In the oxidative ammonolysis of 3-picoline both $V_4O_9$ and $VO_2$(B) were formed during the reaction (*16*). These samples were then also used in the ammoxidation of 3-picoline at a relatively high partial pressure of oxygen (*17*). It was concluded that $V_4O_9$ exhibited a similar selectivity to $V_2O_5$, and that $VO_2$(B) was nonselective. However, the results were affected by the fact that both the specific surface area and the phase composition of the catalysts changed rapidly with time.

It is known that both $V_4O_9$ and $VO_2$(B) can be formed when $V_2O_5$ is reduced by $H_2$, $NH_3$, or organic compounds at relatively low temperatures (483–673 K) (*18*). It was of interest to compare the performances of $V_4O_9$ and $VO_2$(B) with the performance of $V_2O_5$ without having the results influenced by large variations in specific surface area. In this study this was achieved by a proper selection of the reaction parameters. The reactor was loaded with $V_2O_5$ and the activity, selectivity, and composition of the catalyst were followed as a function of time-on-stream at various temperatures. The phase composition of the catalyst varied with these parameters. However, because the specific surface area of the catalyst was almost constant with time-on-stream, this procedure allowed us to directly compare the performances of the reduced oxides in relation to the fresh catalyst, $V_2O_5$. If the reactor is charged with freshly prepared reduced oxides, phase changes can occur during the initial warmup period. Our methodology avoided such startup variations.

Another important object of this investigation was to follow the changes of the catalyst composition with HRTEM (high-resolution transmission electron microscopy). The purpose of this was to clarify the nature of defects and phases formed under the influence of the reaction medium. These studies will also be used to evaluate the accuracy of the structures proposed for $V_4O_9$ (*19*) and $VO_2$(B) (*18*) which will be presented in forthcoming papers. So far no single-crystal studies of these oxides have been reported.

## METHODS

*1. Catalyst preparation.* The freshly prepared catalyst was composed of $V_2O_5$. It was obtained by decomposing $NH_4VO_3$ (Merck p.A.) in a stream of air for 2 h. The temperature was kept relatively low at 673

K in order to obtain a high specific surface area. The surface area was determined to be 10.9 $m^2/g$ in comparison with a normal value of about 4 $m^2/g$ for such catalysts. The fraction at 0.1–0.4 mm was used in the experiments.

*2. Catalytic measurements.* An integral plug flow reactor was used in the measurements. Approximately 10% of the mixture of air and nitrogen was passed through a 3-picoline saturator, which was kept at 340 K. $NH_3$, supplied from a pressure cylinder, was added to the reactant stream before it entered the preheater. The composition of the stream entering the reactor was 3-picoline, 0.44 vol%; $NH_3$, 1.78 vol%; $O_2$, 1.87 vol%; and $N_2$, 95.91 vol%. The product stream passed through a series of condensers and water absorbers. The condensate was dissolved in both water and chloroform, combined with the contents of the absorbers, and then extracted. 2-Picoline was added to the chloroform phase as an internal standard. This phase was analyzed on a Perkin–Elmer F33 gas chromatograph with a FID detector. A 1.5-m column loaded with 30% SE-30 on A.W. Chromosorb W was used at 343 K. To the column was added 1% triethanolamine to prevent tailing (*20*). The water phase was evaporated to dryness, and the weight of high boiling tarry compounds was determined. The amount of $CO_2$ leaving the absorbers was analyzed after absorption in tubes filled with Ascarite and Dehydrite. The amount of $CO_2$ dissolved in the water phase was also determined. This was done gravimetrically after adding $BaCl_2 \cdot 2H_2O$. Ascarite and Dehydrite tubes were also used for the determination of the amount of CO formed. This was possible by first oxidizing the CO to $CO_2$ by passing it through a heated U-tube filled with granular $I_2O_5$.

The reactor was loaded with 1.25 ml of freshly prepared $V_2O_5$. A stream of air was passed through the bed while the catalyst was heated to the reaction temperature. Product analyses were carried out continuously at a fixed reactor temperature. Samples were collected at 10-min intervals. By plotting the conversion and selectivities as a function of time-on-stream, the performance of the freshly prepared catalyst could be determined by extrapolation to initial time. The performance of the lower oxides, which were formed during the course of the reaction, could also be directly compared with the values related to the pure $V_2O_5$ catalyst.

*3. Catalyst characterization.* The X-ray diffraction patterns of both used and freshly prepared catalysts were registered on a Philips X-ray diffraction instrument using a PW 1310/01/01 generator and Cu$K\alpha$ radiation.

Infrared spectra of catalyst samples were recorded on a Perkin–Elmer 297 spectrophotometer. Disks containing 2 mg of sample and 300 mg of KBr were prepared.

A gravimetric BET apparatus was used for determination of the specific surface area. The measurements were made using $N_2$ at liquid $N_2$ temperature. Prior to adsorption the samples were degassed at 523 K for 2 h. The degassing pressure was $5 \times 10^{-3}$ Pa.

The average oxidation number of vanadium was determined by titrimetric methods using potassium permanganate and Mohr's salt (*21*).

The HRTEM investigation was carried out with a JEOL 200CX microscope, equipped with an ultrahigh-resolution top-entry goniometer (THG2) with nominal values for the spherical aberration coefficient ($C_s$) of 1.2 mm, and for the chromatical aberration coefficient ($C_c$) of 1.4 mm at 200 kV. A $LaB_6$ filament was used throughout the investigation. Very thin crystal fragments of the catalyst were suspended in methanol and collected on 3-mm copper grids covered with a holey carbon film. Structure images were recorded at magnifications of 500,000× and 800,000× using an objective lens aperture of 4.5 $nm^{-1}$ and a defocus value close to the Scherzer focus, $\Delta f = -57$ nm. In cases where the crystal structure was known from X-ray diffrac-

tion, experimental images were compared with computersimulated ones obtained using the multislice method.

## RESULTS AND DISCUSSION

### *1. Performance of a $V_2O_5$ Catalyst*

Figure 1 shows the conversion and selectivities for the pure $V_2O_5$ catalyst as a function of temperature. The data were obtained by extrapolating time-on-stream curves to initial time. It is interesting to note that the selectivity for the formation of $CO_2$ passes through a minimum. Exactly the same behavior was observed for a $V_6O_{13}$–$V_2O_4$ catalyst under similar reaction conditions (*8*). The same dependence has also been observed by Haber and Wiltowski in the oxidation of propylene over $CuMoO_4$ (*22*). This behavior indicates the existence of two different types of oxygen species on oxide surfaces. One type is responsible for the formation of $CO_2$ at low temperatures, while a second type takes part in the selective reaction. This second type also participates in the further degradation of the nitrile at high temperatures. These types of oxygen species can be identified by consideration of the literature in the field.

Both $O_2^-$ and $O^-$ species have been observed on a partially reduced $SiO_2$-supported $V_2O_5$ catalyst at temperatures as high as 573 K in an oxygen atmosphere (*23*). On supported catalysts, the $O^-$ species in particular showed a high reactivity even at temperatures as low as 77 K (*24*). These species could not be detected on partially reduced unsupported $V_2O_5$. However, surface potential measurements (*25*) have revealed the existence of both $O_2^-$ and $O^-$ species on pure $V_2O_5$ as well as on $V_2O_5$–$TiO_2$ samples. The kinetics of the potential changes occurring upon the uptake of oxygen were compatible with the existence of $O_2^-$ in the temperature interval 353–453 K and with the existence of $O^-$ in the region 553–643 K. At intermediate temperatures both types of species were present. The $O_2^-$ and $O^-$ species are both strongly electrophilic and attack the organic molecule in the region of its highest electron density (*2*). This attack leads to a degradation of the hydrocarbon molecule and eventually to the formation of total oxidation products. The findings referred to can very well be used to explain the curves shown in Fig. 1. The selectivity for the formation of $CO_2$ is high at 577 K due to the existence of electrophilic $O^-$ species on the surface. When the temperature increases the $CO_2$ selectivity decreases because the surface concentration of weakly bonded $O^-$ species diminishes. At temperatures above 725 K the selectivity for the formation of $CO_2$ again increases. This is due to the fact that the nitrile formed reacts further with lattice $O^{2-}$ species.

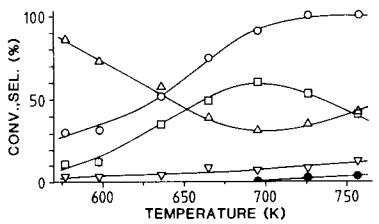


FIG. 1. Conversion and selectivities as a function of temperature for a pure $V_2O_5$ catalyst. Conversion, ○; and selectivity for the formation of nicotinonitrile, □; carbon dioxide, △; carbon monoxide, ●; and tar, ▽.

In a previous investigation of a $V_2O_5$ catalyst in the ammoxidation of 3-picoline a selectivity minimum for the formation of carbon oxides was not observed at any temperature between 573 and 789 K (*4*). This might be due to differences in the plane distribution of the catalysts in the two studies. Recently, the importance of anisotropy in catalysis has been demonstrated (*26–28*). The catalyst used in the previous investigation was prepared by melting $V_2O_5$ and then cooling it to room temperature. After that the cake was crushed. Because of their layered structure $V_2O_5$ crystals are most easily broken parallel to the (010) plane. Thus the use of this method results in particles which preferentially expose the (010) plane. The scanning electron micrographs of this sample clearly revealed the existence of large

(010) planes (*4*). The method of preparation used in the current investigation gives polycrystalline aggregates with a plane distribution which is nearly uncharacterizable by electron microscopy. Therefore, the morphological factor, $f = I_{101}/I_{010}$, defined by Gasior and Machej (*27*) was determined to characterize the two catalyst samples. The value of $I$ is defined as the intensity of the X-ray reflection indexed. Table 1 shows the morphological factors together with some catalytic data. The facts presented clearly show that the exposure of (010) planes is beneficial for the formation of nitrile, and that the formation of $CO_2$ at 600 K cannot be correlated primarily to the frequency of (010) planes. These results are in agreement with those obtained in the oxidation of *o*-xylene on $V_2O_5$ catalysts (*27*). In that case the selectivity for the formation of carbon oxides was 32% for a catalyst with $f = 0.1$ and 55% when $f = 0.6$. In our case no carbon oxides were formed on the molten and crushed catalyst at 600 K, which could be due to coke formation. This is reflected in the $\Sigma$ value in Table 1, which represents the sum of the selectivities.

A more detailed analysis of the X-ray data is given in Table 2. The table includes the relative intensities of the 11 most important reflections. It is obvious that the reflections with indices (00*l*) and (*h*00) are generally more intense in the decomposed nonselective catalyst than in the crushed catalyst. This is interesting since both the (001) plane and the (100) plane are nonselective because of being able to accommodate a high concentration of electrophilic $O^-$ species, which can be demonstrated by making use of the so-called oxidized surface state model (*29*). This model uses bond-strength calculations to calculate charge distributions. The bond strengths ($s$), or the formal valences, around the individual vanadium–oxygen bonds in $V_2O_5$ were calculated by the empirical expression $d = 1.791\text{-}0.722 \log s$, where $d$ is the individual bond length (*30*). The $s$ values are given in Table 3. From these values it can be inferred that the (001) planes are covered with electrophilic oxygen species with $s = 0.76$. A similar situation exists at the (100) plane. However, in this case the positions of the most weakly bonded anions with $s = 0.48$ are probably vacant at high temperatures. The (010) plane exposes both $V^{5+}$ cations and vanadyl groups. Considering

TABLE 1

Dependence of Selectivities on the Morphological Factor

| $V_2O_5$ sample | Selectivity (%) at 600 K | | | | $f$ |
|---|---|---|---|---|---|
| | Nitrile | $CO_2$ | Tar | $\Sigma$ | |
| Crushed | 61 | 0 | 15 | 76 | 0.11 |
| Decomposed | 18 | 73 | 4 | 95 | 1.00 |

TABLE 2

X-Ray Analysis of $V_2O_5$ Catalysts

| Indices (*hkl*) | Cu$K\alpha_1$ *d*(nm) | Crushed $I$(i)/$\Sigma I$(i) | Decomp. $I$(i)/$\Sigma I$(i) |
|---|---|---|---|
| 200 | 0.576 | 0.050 | 0.048 |
| 010 | 0.438 | 0.525 | 0.163 |
| 110 | 0.409 | 0.116 | 0.059 |
| 101 | 0.340 | 0.055 | 0.168 |
| 400 | 0.288 | 0.098 | 0.159 |
| 011 | 0.276 | 0.028 | 0.072 |
| 301 | 0.261 | 0.028 | 0.090 |
| 600 | 0.192 | 0.038 | 0.071 |
| 021 | 0.186 | 0.020 | 0.048 |
| 002 | 0.178 | 0.026 | 0.084 |
| 610 | 0.176 | 0.016 | 0.038 |

TABLE 3

Electron Delocalization around V–O Bonds in $V_2O_5$

| Plane (*hkl*) | Bond length[a] (nm) | Bond strength, $s$ ($e^-$) |
|---|---|---|
| 100 | 1 × 0.2021 | 0.48 |
| 100 | 1 × 0.1780 | 1.04 |
| 010 | 1 × 0.1585 | 1.93 |
| 010 | 1 × 0.2785 | 0.04 |
| 001 | 2 × 0.1878 | 0.76 |

[a] From Bachmann *et al.* (*31*).

the $V_2O_5$ structure it follows that in principle every plane except the (010) plane can accommodate a certain amount of electrophilic oxygen species.

Another explanation for total combustion preferentially occurring at the (100) and (001) planes, or at the (101) planes, has been presented by Haber (*32*). In this case it is stated that shear planes are nucleated at the (101) planes, or (100) and (001) planes, and that whole perpendicular layers of oxygen can be extracted resulting in total combustion. The oxidized surface state model complements this picture by showing that the anions on these planes are highly electrophilic.

### 2. *Infrared Spectra of Catalysts*

Figure 2 presents the infrared spectra of both used and unused catalysts. The unused catalyst exhibits the infrared spectrum of pure $V_2O_5$. The peak at 1022 $cm^{-1}$ is associated with the symmetric stretching vibrations of vanadyl groups, while the bands at 824 and 608 $cm^{-1}$ correspond to asymmetric and symmetric stretching vibrations, respectively, of V–O–V units having bridged, 2-coordinated, oxygen species (*33*). When the catalyst had been used at 665 K its infrared spectrum was that of pure $V_4O_9$. Typical for this spectrum is the broadband at 920–930 $cm^{-1}$, which seems to be composed of several sharp peaks. All of the modes appearing at 1028, 980, 952, 928, 905, 885, 848, 805 (very weak), and 718 $cm^{-1}$ are relevant for $V_4O_9$ (*34, 35*). After use at 598 K the spectrum was that of a mixture of $V_2O_5$ and $V_4O_9$. The spectrum for 636 K also shows some background features originating from a weak $V_2O_5$ spectrum. After the reaction was carried out at 695 and 726 K the spectrum developed a strong broadband at 922 $cm^{-1}$ and additional weak bands at 1005 and 725 $cm^{-1}$. A broadband also seems to appear around 600 $cm^{-1}$. The same infrared modes appear to have been observed by Théobald (*34*) for $VO_2$(B), even though the spectrum in that case was much less well resolved. No infrared bands appeared after use at the highest temperature investigated, 757 K.

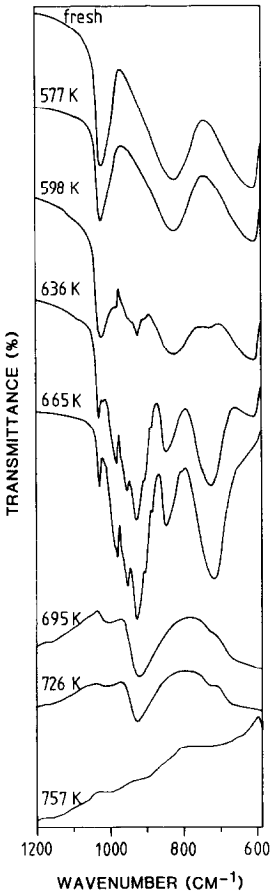


FIG. 2. Infrared spectra of catalysts after 40 min on stream at various temperatures.

### 3. *HRTEM Studies of Catalysts*

Catalysts, both freshly prepared and after 40 min on stream, were characterized by HRTEM. Crystals of the unused catalyst which were investigated showed structure images of $V_2O_5$ like that in Fig. 3. Structural defects such as twin lamellae (*36, 37*) could not be found in the crystals of the unused catalyst. The electron diffractograms gave no indications of any atom displacements. The contrast variations in the image of Fig. 3 can be explained as crystal thickness variations.

The catalyst used at 598 K was composed mainly of $V_2O_5$ crystals, but a significant

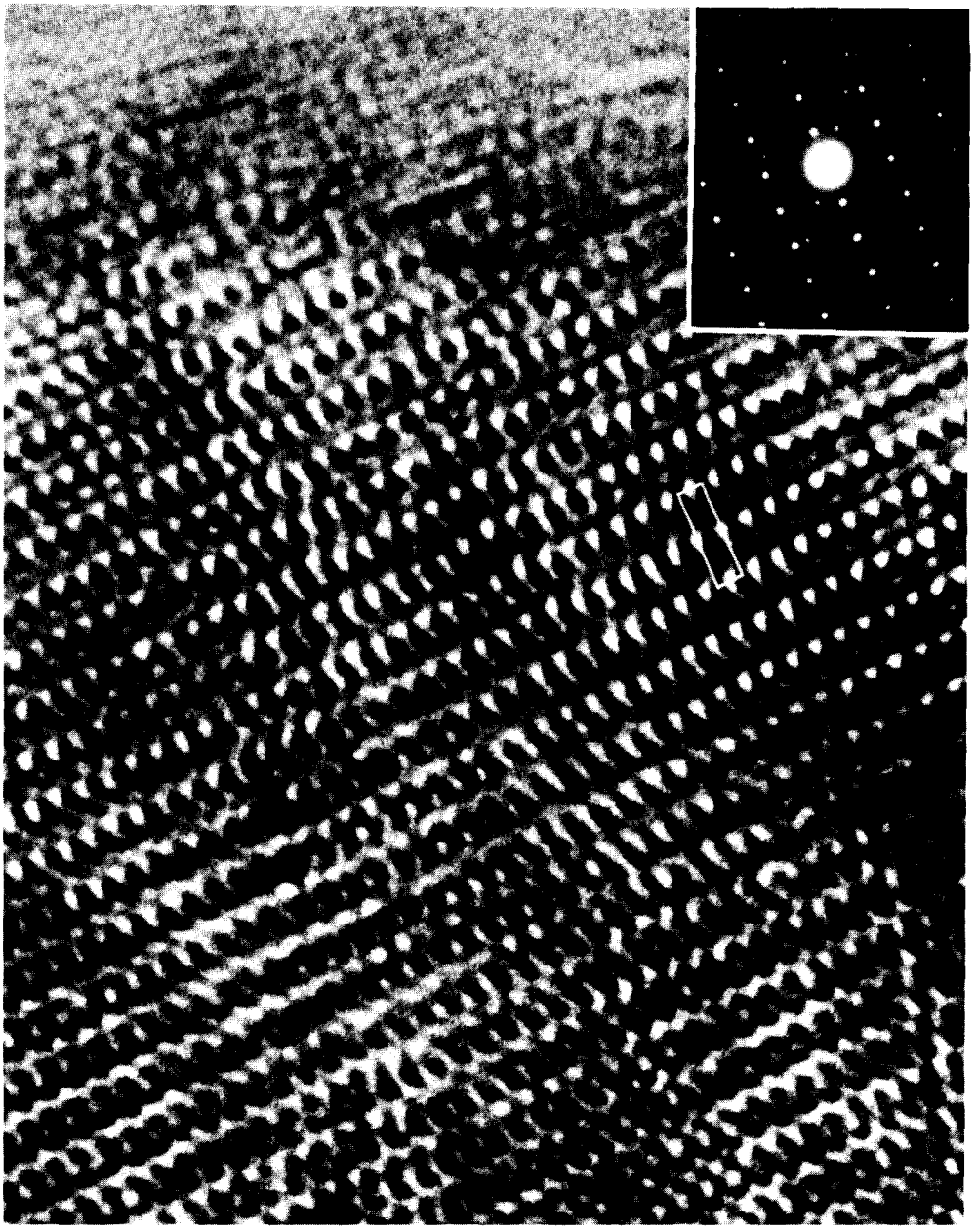

FIG. 3. Crystal structure image of a $V_2O_5$ crystal recorded with the electron beam parallel to [010]. The unit cell, $a$ = 1.151 nm and $c$ = 0.356 nm, is marked and the corresponding electron diffraction pattern is inserted.

amount of $V_4O_9$ crystals ($a$ = 0.824 nm, $b$ = 1.032 nm, and $c$ = 1.647 nm) (*19*) was also found. It was obvious from the HRTEM images that $V_2O_5$ crystals could be partly reduced to a $V_4O_9$ phase as shown in Fig. 4. This crystal structure image, projected along ⟨010⟩ of $V_2O_5$, shows an ideal structure image of $V_2O_5$ in the lower left part while the upper right part shows a well-ordered $V_4O_9$ structure image with $a$ = 0.813 nm and $b$ = 1.041 nm along ⟨001⟩. Viewing the image at a low angle along ⟨001⟩ of

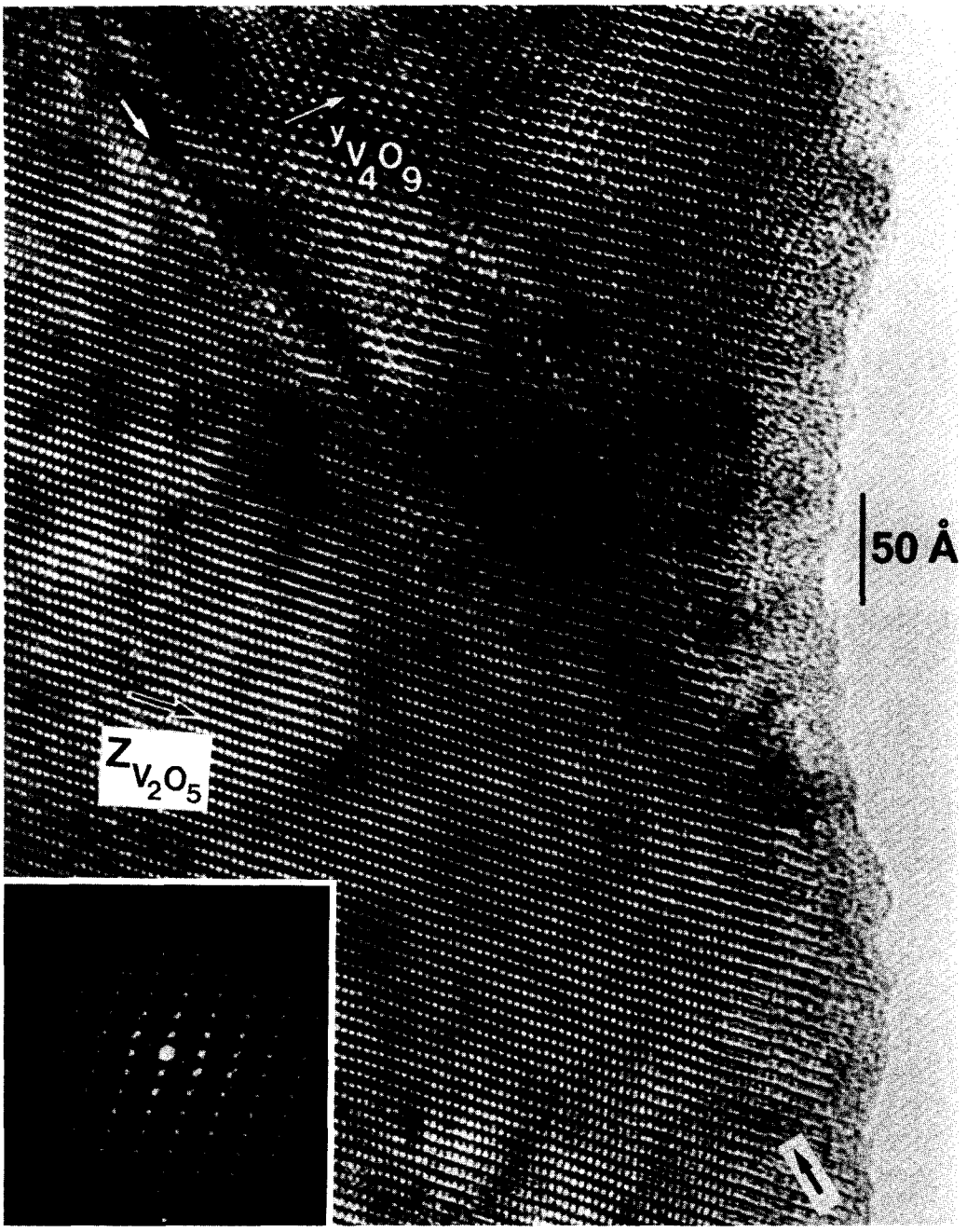


FIG. 4. High-resolution electron micrograph of the phase boundary (diagonal arrows) between $V_2O_5$ (lower left) and $V_4O_9$ (upper right). The electron beam was parallel to [010] and [001] of $V_2O_5$ and $V_4O_9$, respectively. The electron diffractogram inserted shows the reflections of both phases. The $V_4O_9$ reflections are the weaker ones.

$V_2O_5$, marked with an arrow, reveals a discontinuity in the structure along the border (diagonal arrows) between $V_2O_5$ and $V_4O_9$. The angle between ⟨001⟩ of $V_2O_5$ and ⟨110⟩ of $V_4O_9$ can be estimated to be approximately 4.5° from the electron diffractogram. This value was found to range from 2.7 to 4.7° in different crystals investigated.

The general direction of the phase boundary between $V_2O_5$ and $V_4O_9$ is parallel to the (301) plane of $V_2O_5$. However, it is not certain that the phase boundary is actually planar; it could just as well be curved as indicated by the uneven contrast of the regions around the boundary, especially in the thicker part of the crystal. If the edge of the crystal imaged was on the surface of the catalyst particle, which seems most likely, the reduction of $V_2O_5$ to $V_4O_9$ would appear to proceed from the surface.

The catalyst used at 636 K consisted mainly of $V_4O_9$ crystals, but a few crystals of $V_2O_5$ were still found by HRTEM. Some crystals contained islands of $V_2O_5$ in a matrix of $V_4O_9$ as shown in Fig. 5. This is unique and very characteristic for this temperature. As judged from the image, the $V_2O_5$ domains (A) could be as small as 2 nm. It can be concluded that the reduction of $V_2O_5$ can start a structural rearrangement to the structure of $V_4O_9$ in two different orientations, because the crystal in Fig. 5 shows $V_4O_9$ structure units of different orientations. The two units are twin oriented to each other over the (110) plane, which is marked with the large arrow. This is also obvious from consideration of the electron diffractogram.

Crystals of $VO_2$(B) dominated the sample used in the reaction at 695 K. A few crystals of $V_6O_{13}$ and monoclinic $VO_2$ were also found by HRTEM. Characteristic structural features of the $VO_2$(B) crystals were planar twin lamellae of two new types. One

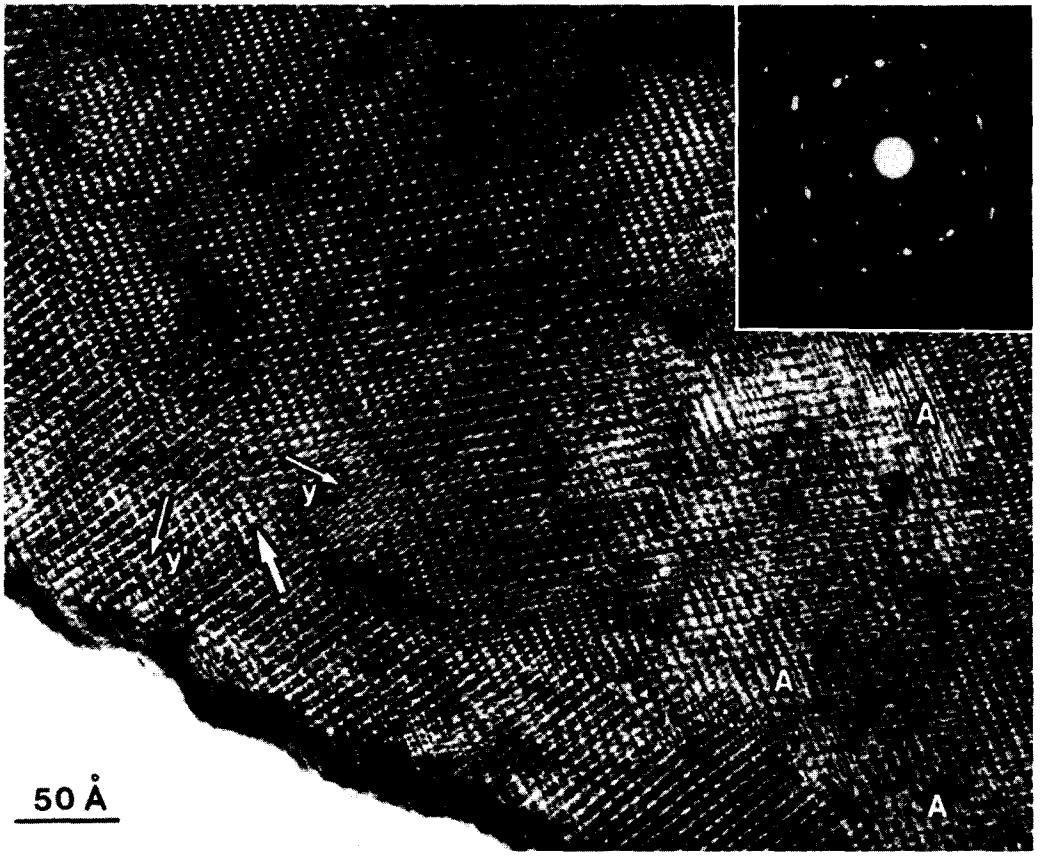


FIG. 5. Electron micrograph and diffractogram of twin oriented $V_4O_9$ regions in a crystal also containing small $V_2O_5$ islands (A). The electron beam was parallel to [001] of $V_4O_9$. A twin boundary (110) is marked with a large arrow.

type appeared in the ⟨001⟩ projection as a very narrow twin lamella of (410) twin planes. This lamella is shown in Fig. 6 and is only 1.2 nm broad. The other type of twin lamella is made up of parallel (201) planes as shown in Fig. 7. The distance between the twin planes is 6 nm in this case. The crystal structure of $VO_2$(B) has not yet been determined by single-crystal X-ray diffraction. Crystal structure images and the nature of the defects will contribute to a structure determination by HRTEM (*38*).

After the catalyst was used at 726 K $VO_2$(B) was found with a minor amount of monoclinic $VO_2$ present. The structural defects of the $VO_2$(B) crystals formed at this temperature showed a somewhat different structure compared to those of the sample

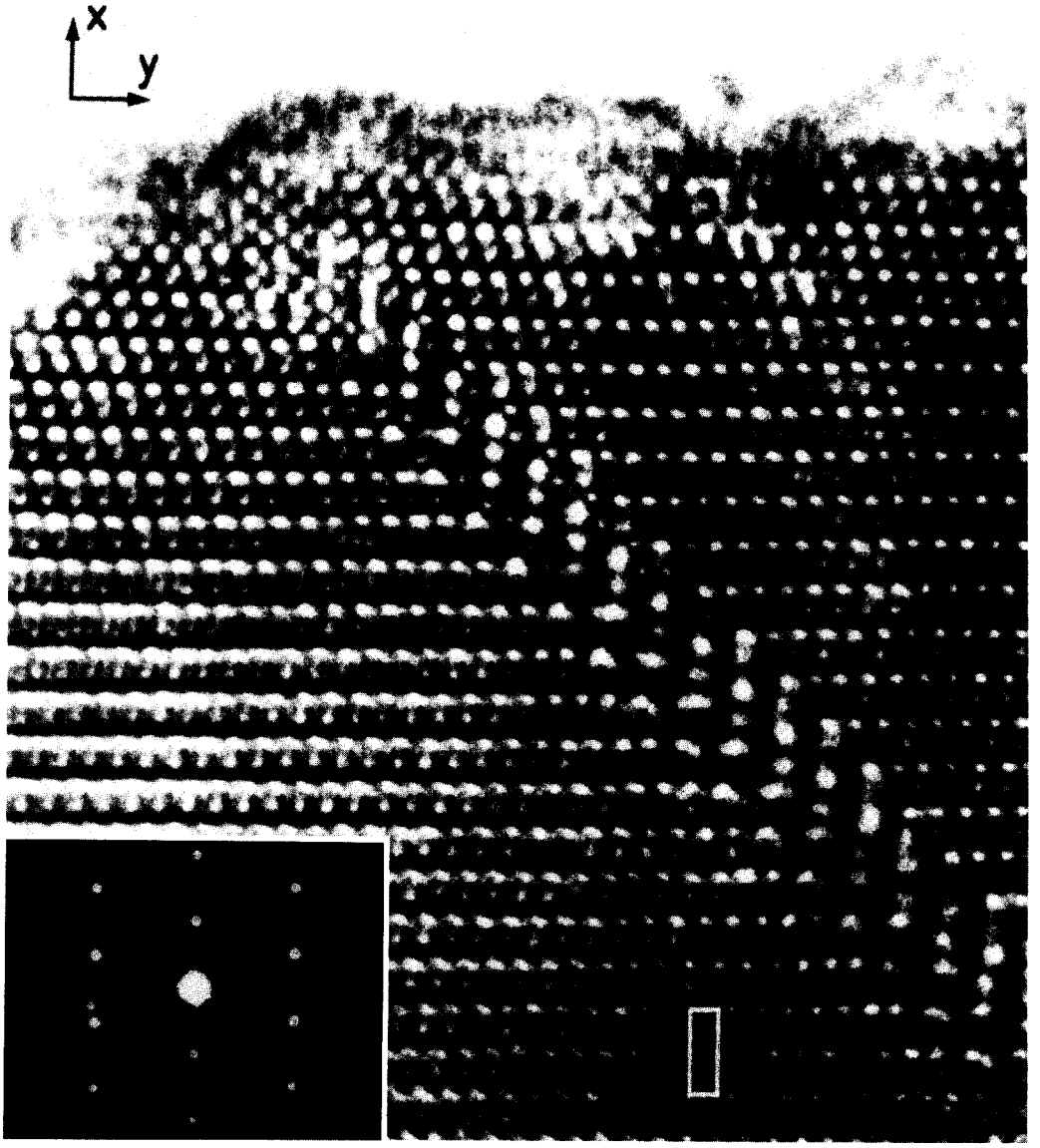


FIG. 6. Crystal structure image of a $VO_2$(B) crystal recorded along [001]. The (410) twin planes constitute a 1.2-nm broad twin lamella defect. The unit cell is marked and the electron diffractogram is inserted.

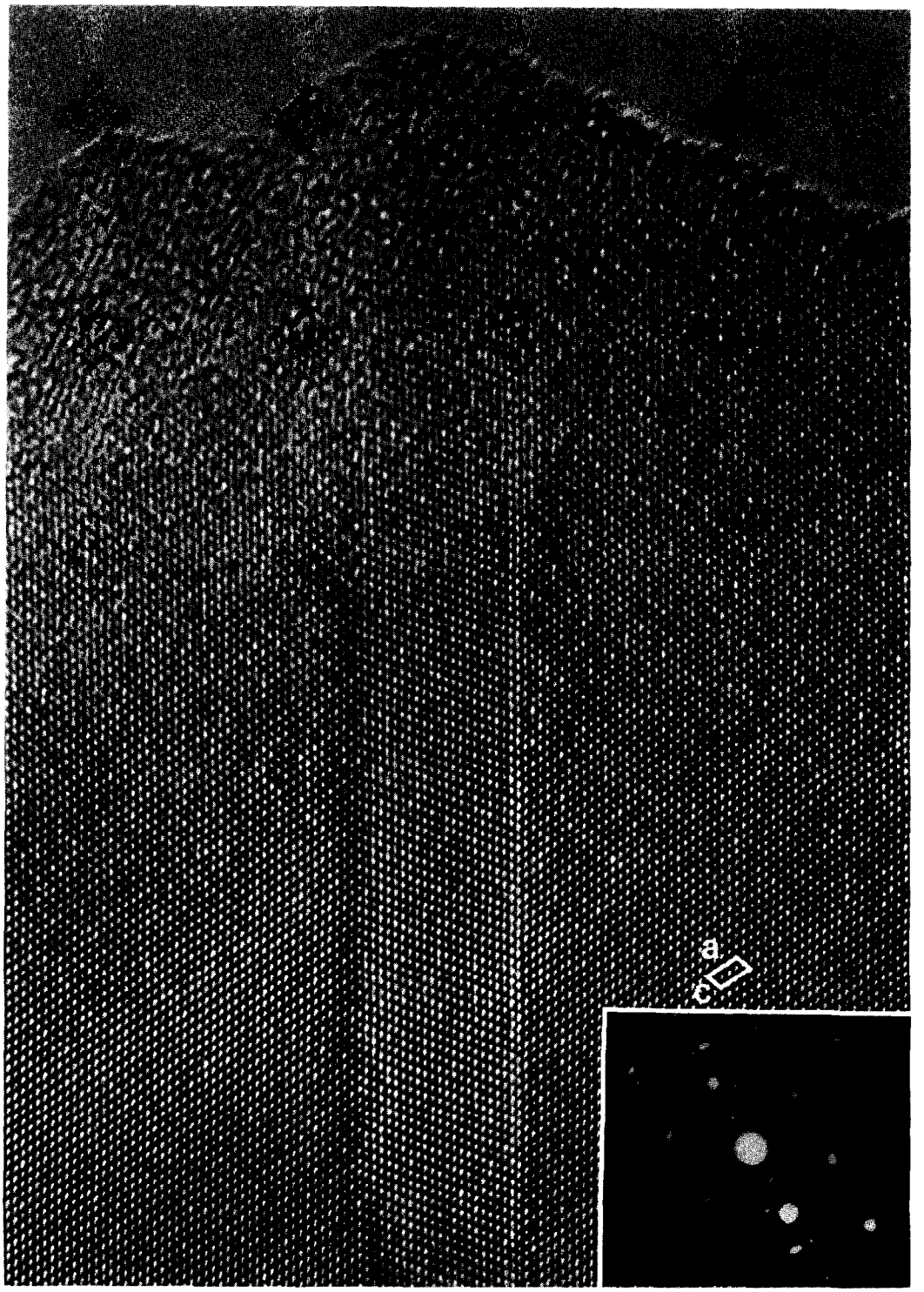


FIG. 7. Crystal structure image of a $VO_2$(B) crystal recorded along [010]. The twin lamella is 6 nm broad and the twin planes are parallel to (201). The experimental cell parameters $a = 1.18$ nm and $c = 0.64$ nm are marked and the electron diffractogram is inserted.

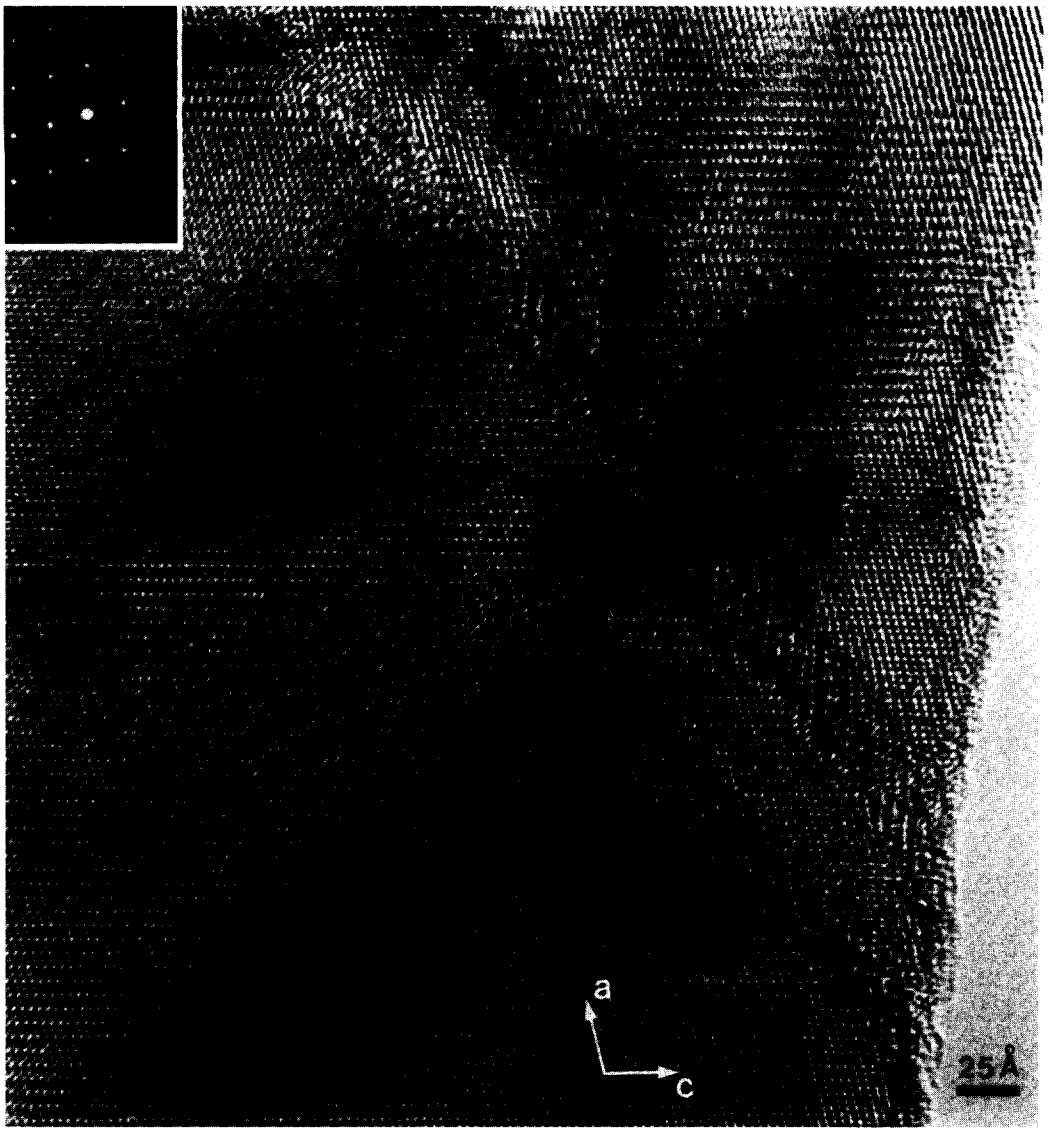


FIG. 8. Electron micrograph and diffractogram of a $VO_2$(B) crystal. The electron beam was parallel to [010].

reacted at 695 K. The image of the crystal in Fig. 8 reveals that the defects were partly amorphous and terminated in the crystal. The general direction of the borders of the defects is approximately parallel to (101) of the $VO_2$(B) crystal matrix. This investigation shows that the nature of defects developed in $VO_2$(B) depends on the reactor temperature.

The structure of the catalyst used at 757 K was very complex. The crystals contained several phases of various orientations, which were unidentifiable by HR-TEM. Electron diffraction patterns of sufficiently small areas of the crystals could not be obtained because the electron beam diameter of the JEOL 200CX instrument is too large.

### *4. Average Oxidation Number*

Figure 9 shows the average oxidation number of vanadium after the catalyst was used at various temperatures. It is obvious

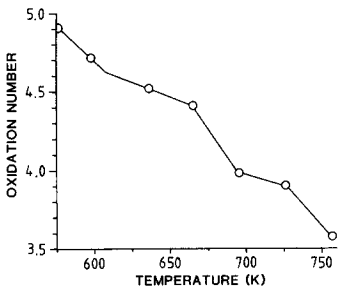


FIG. 9. Average oxidation number of vanadium after 40 min on stream as a function of the reaction temperature.

that the catalyst became more reduced as reaction temperature rose. What is interesting is that the curve seems to level out around the values 4.5 and 4. This is due to the stability of the $V_4O_9$ and $VO_2$ phases.

### 5. *X-Ray Characterization*

In addition to HRTEM and IR spectroscopy the catalysts were also characterized by X-ray diffraction. Table 4 includes the main phases identified by the various methods. It can be seen that $V_2O_5$ is first reduced to $V_4O_9$ and then to $VO_2$(B) and tetragonal $VO_2$ (monoclinic at room temperature) as a function of reaction temperature. Finally, at high temperatures, additional lower oxides are formed. It is worth mentioning that no $V_3O_7$ (*11*) was found in any catalyst sample. At 665 and 695 K the catalyst was composed of almost pure $V_4O_9$ or $VO_2$(B), respectively. The 10 most intense X-ray lines of these catalysts are collected in Table 5. The positions of the lines agree with data published by Théobald *et al.* (*12, 13*). However, due to different plane distributions the relative intensities differ somewhat. Another $V_4O_9$ structure has been determined by Wilhelmi and Waltersson (*39*). This phase, which was later suggested to have the composition $V_4O_8$(OH) (*40*), was not discovered in any catalyst sample. After use at 757 K the X-ray pattern, in addition to the lines of $VO_2$, also had some lines at positions corresponding to $V_4O_7$ (*41*) and $V_2O_3$. Besides $V_4O_7$, any additional Magnéli phase $V_nO_{2n-1}$ (*42*) could not be detected.

### 6. *Performance after 40 min on Stream*

The performance of the freshly prepared $V_2O_5$ catalyst was followed during the initial 40 min at each temperature studied. The conversion and selectivities varied with time-on-stream, and as an example a plot for 695 K is shown in Fig. 10. Similar curves were drawn for each temperature. The results obtained are summarized in Table 4, where the conversion and selectivities measured after 40 min on stream can be directly compared with the values of the freshly prepared $V_2O_5$ catalyst. In the last column the values of the specific surface

TABLE 4

Dependence of Conversion, Selectivity, and Catalyst Composition upon Time-on-Stream

| Reaction temperature (K) | Initial time, $t$ = 0 min | | | Time-on-stream, $t$ = 40 min | | | | |
|---|---|---|---|---|---|---|---|---|
| | Conversion (%) | Selectivity (%) | | Conversion (%) | Selectivity (%) | | Phase comp. | Surface area ($m^2/g$) |
| | | Nitrile | $CO_x$ | | Nitrile | $CO_x$ | | |
| 577 | 30.6 | 11.5 | 86.9 | 25.2 | 8.7 | 85.7 | $V_2O_5$ | 10.1 |
| 598 | 31.8 | 12.8 | 73.4 | 26.3 | 9.5 | 79.8 | $V_2O_5$, $V_4O_9$ | 12.5 |
| 636 | 52.2 | 35.6 | 57.7 | 49.9 | 26.0 | 69.7 | $V_4O_9$, ($V_2O_5$) | 10.9 |
| 665 | 75.0 | 48.4 | 39.5 | 63.2 | 41.6 | 55.4 | $V_4O_9$ | 11.7 |
| 695 | 90.7 | 60.2 | 32.0 | 98.5 | 35.8 | 58.3 | $VO_2$(B) | 11.8 |
| 726 | 100 | 53.2 | 38.5 | 100 | 57.1 | 34.7 | $VO_2$(B), ($VO_2$) | 12.0 |
| 757 | 100 | 41.1 | 46.8 | 92.3 | 53.1 | 34.1 | $VO_2$,$V_4O_7$,$V_2O_3$ | 13.0 |

TABLE 5

X-Ray Lines of the $V_4O_9$ and $VO_2$(B) Phases Formed during the Catalytic Reaction

| $V_4O_9$—665 K | | $VO_2$(B)—695 K | |
|---|---|---|---|
| $d$(nm) | $I/I_0$ | $d$(nm) | $I/I_0$ |
| 0.321 | 100 | 0.205 | 100 |
| 0.414 | 72 | 0.201 | 90 |
| 0.165 | 64 | 0.185 | 78 |
| 0.319 | 58 | 0.156 | 73 |
| 0.254 | 48 | 0.351 | 62 |
| 0.173 | 42 | 0.170 | 41 |
| 0.159 | 33 | 0.158 | 37 |
| 0.207 | 32 | 0.266 | 35 |
| 0.203 | 31 | 0.297 | 33 |
| 0.213 | 29 | 0.307 | 32 |

area are given for the used catalysts. The differences between the surface areas of the used catalysts and the fresh catalyst, which had a value of 10.9 $m^2/g$, are rather small.

A comparison of data given in Table 4 provides evidence that $V_4O_9$ is both less active and less selective than pure $V_2O_5$. The $V_2O_5/V_4O_9$ phase boundaries present in the samples used at 598 and 636 K (Figs. 4 and 5) do not exhibit any decisive effects on either the activity or the selectivity. Baiker and Zollinger (*17*) reported $V_4O_9$ to be as active and selective as $V_2O_5$ in the ammoxidation of 3-picoline when using a larger oxygen/3-picoline ratio. This might depend on a rearrangement of the $V_4O_9$ surface.

The data obtained for $VO_2$(B) at 695 K show that this phase is more active but less selective than $V_2O_5$. Its relatively low selectivity for the formation of nitrile seems not to be an effect of the high level of conversion obtained, because even at 726 K, $V_2O_5$ at 100% conversion gives a selectivity of 53%.

At 726 K X-ray and electron diffraction data indicate the coexistence of both $VO_2$(B) and tetragonal $VO_2$ after 40 min on stream. This two-component catalyst was even more selective than pure $V_2O_5$ at the same conversion, a fact which cannot be explained by a linear combination of the performances of the two constituent oxides. It has been concluded that $VO_2$(B) is not selective and tetragonal $VO_2$ has been found to be inactive in the ammoxidation of 3-picoline (4). Therefore, in this case it seems that the high activity and selectivity could be due either to the phase boundaries themselves or to other types of defects present, e.g., partly amorphous defects of the type shown in Fig. 8.

At 757 K the conversion decreased and the selectivity for the formation of nitrile increased with time-on-stream. Simultaneously, tetragonal $VO_2$, $V_4O_7$, and $V_2O_3$ were formed. It is obvious that a multicomponent system like this must exhibit a number of structural defects and phase boundaries. However, it was not possible to characterize them by the use of HRTEM. Any decisive conclusions about their influence on the catalytic reaction cannot be drawn without further investigations. $V_2O_3$ has been found to be inactive in the oxidation of *o*-xylene (*9*), but has been reported as being active in the oxidation of naphthalene (*10*). However, this fact was inferred as being dependent on a reconstruction of the original surface. So far no reports of the

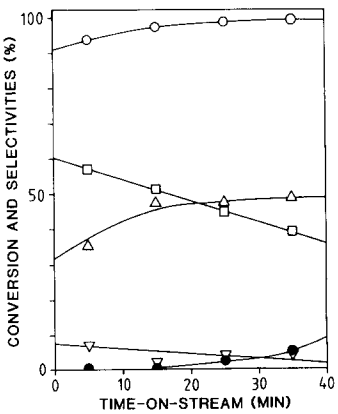


FIG. 10. Conversion and selectivities at 695 K as a function of time-on-stream. Conversion, ○, and selectivity for the formation of nicotinonitrile, □; carbon dioxide, △; carbon monoxide, ●; and tar, ▽.

catalytic activity of $V_4O_7$ seem to have appeared.

In the oxidative ammonolysis, i.e, ammoxidation without molecular oxygen, it was found that both $V_4O_9$ and particularly $VO_2$(B) exhibited a low activity and selectivity in comparison with $V_2O_5$ (*16*). Concerning $V_4O_9$, our investigation shows this result to be valid in the presence of molecular oxygen as well. However, $VO_2$(B) was found to be relatively much more active in ammoxidation than it was reported to be in ammonolysis. This reveals the importance of having molecular oxygen present in the gas phase for the replenishment of the catalyst surface.

In previous investigations of the ammoxidation of 3-picoline it was reported that $V_6O_{13}$ was more active and selective than either $V_2O_5$ (*4*) or $V_4O_9$ (*8*). Combining these facts with the new results presented makes it possible to conclude that the sequence of activity is as follows: $V_6O_{13}$, $VO_2$(B) > $V_2O_5$ > $V_4O_9$ > $VO_2$ (tetragonal). When considering data on the selectivity for the formation of nitrile the sequence is $V_6O_{13}$ > $V_2O_5$ > $V_4O_9$ > $VO_2$(B). These series of activity and selectivity show that $V_6O_{13}$ and $V_2O_5$ are the two most active and selective phases. The catalytic performances of $V_2O_5$, $V_6O_{13}$, and $VO_2$ (tetragonal) in relation to their surface structures have been thoroughly discussed in previous articles (*29, 43*). Similar considerations for $V_4O_9$ and $VO_2$(B) cannot be presented until the crystal structures of these phases have been accurately determined.

It has been observed that the presence of a nonstoichiometric $V_6O_{13}$ phase having an excess of oxygen is especially beneficial for the production of nicotinonitrile (*8, 44*). Recently, it has been possible to image this active and selective phase by HRTEM. It was found to be a grossly amorphous $V_6O_{13}$ phase with short-range order (*45*). The relatively selective catalyst obtained at 726 K in the current investigation was also found to be partly amorphous. However, it is too early to draw any general conclusions about the importance of amorphous states in heterogeneous catalysis.

Our investigation shows that the selective ammoxidation of 3-picoline to nicotinonitrile over $V_2O_5$ can be related to the presence of the (010) plane, which exposes double-bonded oxygen species. On condition that the rate-limiting step in the mechanism involves abstracting hydrogen from the methyl carbon atom, this finding agrees with the suggestion that metal–oxygen double bonds in oxides and molybdates are responsible for the dehydrogenating power of these catalysts (*46*). Infrared bands in the range 900–1100 $cm^{-1}$ have been ascribed to stretching vibrations of metal–oxygen double bonds (*47*). Looking at the infrared spectra presented in Fig. 2 it is seen that the spectra of $V_2O_5$, $V_4O_9$, and $VO_2$(B) all have bands within this range. It has been reported that the $V_6O_{13}$ spectrum has a band very close to this range at 885 $cm^{-1}$, while the spectrum of tetragonal $VO_2$ has no band maximum above 700 $cm^{-1}$ (*44*). Considering the selectivity data and the sequence of selectivity it can be concluded that all oxides presenting any infrared band between 885 $cm^{-1}$ and higher wavenumbers also show selectivity for the formation of nicotinonitrile. $VO_2$ (tetragonal) is neither selective nor active in the ammoxidation of 3-picoline and also does not have any infrared band in the double bond region. These results do not contradict the proposal that double-bonded oxygen species are involved in the dehydrogenating step of catalytic oxidation and ammoxidation. However, no direct correlation between the infrared double bond frequencies of the oxides and their sequence of selectivity can be found. Nor can any easy correlation between frequencies and activities be made. This could be due to the fact that the frequencies registered are related to the bulk of the oxides. The frequencies of the crystallographically corresponding metal–oxygen vibrations at the surface can differ, and also the situation at the surface is far more complex. Geometric factors, competing reactions, and the

existence of electrophilic oxygen species cannot be neglected.

## CONCLUSIONS

The formation of nicotinonitrile in the ammoxidation of 3-picoline over $V_2O_5$ is related to the frequency of (010) planes. Calculations of formal valences have been performed in order to localize crystallographically the positions of electrophilic oxygen species. It is specifically demonstrated that the (100) and (001) planes can accommodate $O^-$ species. However, such species can exist on every plane except the (010) plane. Selectivity data of a $V_2O_5$ catalyst exposing a relatively low concentration of (010) planes show that this catalyst is nonselective at low temperatures. $CO_2$ is the main product. This result is in favor of the conclusions drawn on the crystallographic localization of positions being able to accommodate $O^-$ species.

When comparing the performances of various vanadium oxides in the ammoxidation of 3-picoline, the following sequence of activity can be concluded: $V_6O_{13}$, $VO_2$(B) > $V_2O_5$ > $V_4O_9$ > $VO_2$ (tetragonal). The order of selectivity for the formation of nicotinonitrile is $V_6O_{13}$ > $V_2O_5$ > $V_4O_9$ > $VO_2$(B). Each of the selective oxides has at least one infrared band in the metal–oxygen double bond region. Therefore, it cannot be excluded that vanadyl oxygen species take part in the ammoxidation mechanism. However, no obvious correlation was found between wavenumbers and sequence of selectivity or activity. Activity measurements in some cases also revealed catalytic effects due to crystallographic defects and/or phase boundaries.

High-resolution transmission electron microscopy images show that $V_2O_5$ crystals can be partly reduced to a $V_4O_9$ phase. However, activity measurements on such samples did not indicate any synergetic effects. For $VO_2$(B), images show that the type of defects formed under the action of the reaction medium is temperature dependent. Amorphous defects were found in a $VO_2$ catalyst after use at 726 K. This catalyst is found to be more selective than a $V_2O_5$ sample at the same temperature and conversion. This might be tentative evidence for a beneficial effect in catalysis of the amorphous state since amorphous $V_6O_{13}$ has also been reported to be especially selective for the formation of nicotinonitrile (*45*).

## ACKNOWLEDGMENT

The authors gratefully acknowledge financial support from the National Swedish Board for Technical Development (STU).

## REFERENCES

1. Beschke, H., Friedrich, H., Schaefer, H., and Schreyer, G., *Chem. Z.* **101,** 384 (1977).
2. Haber, J., *in* "Surface Properties and Catalysis by Non-Metals" (J. P. Bonnelle, B. Delmon, and E. Derouane, Eds.), NATO ASI Series, Ser. C, No. 105, p. 1. Reidel, Dordrecht, 1983.
3. Andersson, A., *J. Catal.* **69,** 465 (1981).
4. Andersson, A., and Lundin, S. T., *J. Catal.* **58,** 383 (1979).
5. Colpaert, M. N., *Z. Phys. Chem.* **84,** 150 (1973).
6. Gasior, M., Grzybowska, B., Haber, J., Machej, T., and Ziołkowski, J., *J. Catal.* **58,** 15 (1979).
7. Andersson, A., and Lundin, S. T., *J. Catal.* **65,** 9 (1980).
8. Andersson, A., Wallenberg, R., Lundin, S. T., and Bovin, J.-O., *in* "Proceedings, International Congress on Catalysis, 8th (Berlin 1984)," Vol. V, p. 381. Verlag Chemie, Weinheim, 1984.
9. Simard, G. L., Steger, J. F., Arnott, R. J., and Siegel, L. A., *Ind. Eng. Chem.* **47,** 1424 (1955).
10. Shaprinskaya, T. M., Korneichuk, G. P., and Stasevich, V. P., *Kinet. Katal.* **11,** 139 (1970).
11. Waltersson, K., Forslund, B., Wilhelmi, K.-A., Andersson, S., and Galy, J., *Acta Crystallogr. B* **30,** 2644 (1974).
12. Théobald, F., Cabala, R., and Bernard, J., *C.R. Acad. Sci. Paris Ser. C* **269,** 1209 (1969).
13. Théobald, F., and Bernard, J., *C.R. Acad. Sci. Paris Ser. C* **268,** 60 (1969).
14. Srivastava, R. D., Stiles, A. B., and Jones, G. A., *J. Catal.* **77,** 192 (1982).
15. Fiermans, L., Vandenbroucke, L., van den Berghe, R., and Vennik, J., *J. Microsc. Spectrosc. Electron* **4,** 543 (1979).
16. Baiker, A., and Zollinger, P., *in* "Proceedings, International Congress on Catalysis, 8th (Berlin 1984)," Vol. V, p. 463. Verlag Chemie, Weinheim, 1984.

17. Baiker, A., and Zollinger, P., *Appl. Catal.* **10,** 231 (1984).
18. Théobald, F., Cabala, R., and Bernard, J., *J. Solid State Chem.* **17,** 431 (1976).
19. Grymonprez, G., Fiermans, L., and Vennik, J., *Acta Crystallogr. A* **33,** 834 (1977).
20. Van der Meeren, A. A. F., and Verhaar, A. L. Th., *Anal. Chim. Acta* **40,** 343 (1968).
21. Nakamura, M., Kawai, K., and Fujiwara, Y., *J. Catal.* **34,** 345 (1974).
22. Haber, J., and Wiltowski, T., *Bull. Acad. Pol. Sci. Ser. Sci. Chim.* **27,** 785 (1979).
23. Shvets, V. A., Vorotinzev, V. M., and Kazansky, V. B., *J. Catal.* **15,** 214 (1969).
24. Shvets, V. A., and Kazansky, V. B., *J. Catal.* **25,** 123 (1972).
25. Grzybowska, B., Barbaux, V., and Bonnelle, J.-P., *J. Chem. Res. (M),* 650 (1981).
26. Ziołkowski, J., *J. Catal.* **84,** 317 (1983).
27. Gasior, M., and Machej, T., *J. Catal.* **83,** 472 (1983).
28. Tatibouet, J. M., Germain, J. E., and Volta, J. C., *J. Catal.* **82,** 240 (1983).
29. Andersson, A., *J. Solid State Chem.* **42,** 263 (1982).
30. Waltersson, K., *Chem. Commun. Univ. Stockholm* **7** (1976).
31. Bachmann, H. G., Ahmed, F. R., and Barnes, W. H., *Z. Kristallogr.* **115,** 110 (1961).
32. Haber, J., *in* "Proceedings, International Congress on Catalysis, 8th (Berlin 1984)," Vol. I, p. 85. Verlag Chemie, Weinheim, 1984.
33. Abello, L., Husson, E., Repelin, Y., and Lucazeau, G., *Spectrochim. Acta Part A* **39,** 641 (1983).
34. Théobald, F., *Rev. Roum. Chim.* **23,** 887 (1978).
35. Clauws, P., *Verhand. K. Acad. Wet. Lett. Schone, Kunsten Belg. Kl. Wet.* **42,** 159 (1980).
36. Hyde, B. G., and Tilley, R. J. D., *Phys. Status Solidi A* **2,** 749 (1970).
37. Andersson, A., Bovin, J.-O., and Lundin, S. T., *in* "Proceedings, International Congress on Electron Microscopy, 10th (Hamburg, 1982)," Vol. 2, p. 51. Deutsche Gesellschaft für Elektronenmikroskopie, Frankfurt, 1982.
38. Andersson, A., and Bovin, J.-O., to be published.
39. Wilhelmi, K.-A., and Waltersson, K., *Acta Chem. Scand.* **24,** 3409 (1970).
40. Casalot, A., *Mater. Res. Bull.* **7,** 903 (1972).
41. Andersson, S., and Jahnberg, L., *Ark. Kemi* **21,** 413 (1964).
42. Horiuchi, H., Tokonami, M., Morimoto, N., Nagasawa, K., Bando, Y., and Takada, T., *Mater. Res. Bull.* **6,** 833 (1971).
43. Andersson, A., *in* "Studies in Surface Science and Catalysis" (M. Che and G. C. Bond, Eds.), Vol. 21, p. 381. Elsevier, Amsterdam, 1985.
44. Andersson, A., *J. Catal.* **76,** 144 (1982).
45. Andersson, A., and Bovin, J.-O., *Naturwissenschaften* **72,** 209 (1985).
46. Trifirò, F., and Pasquon, I., *J. Catal.* **12,** 412 (1968).
47. Barraclough, C. G., Lewis, J., and Nyholm, R. S., *J. Chem. Soc.,* 3552 (1959).